Journal of
Marine Science and Engineering

MDPI

Article

A Simplified Calculation Method for Cyclic Response of Laterally Loaded Piles Based on Strain Wedge Model in Soft Clay

Xin Liu [1], Zhongyuan Yao [2], Wenbo Zhu [3,*], Yu Zhang [2], Shu Yan [1], Xiaojiang Guo [1] and Guoliang Dai [3]

1 Huaneng Clean Energy Research Institute, Beijing 102209, China
2 Shengdong Rudong Offshore Wind Power Co., Ltd., Nantong 226000, China
3 School of Civil Engineering, Southeast University, Nanjing 211189, China
* Correspondence: 230169390@seu.edu.cn

Abstract: This paper proposed a simplified calculation method to analyze the cyclic response of large-diameter single piles based on the modified strain wedge model. Firstly, the pile–soft clay interaction above the pile-rotating point is represented by a *p–y* curve, and the pile–soft clay interaction below the rotating point is represented by an equivalent rotation spring. At the same time, a stiffness attenuation model is proposed to describe the cyclic *p–y* curve for analyzing the cyclic bearing characteristics of soft clay. Finally, the simplified calculation method is verified by two case studies. The results from the proposed method agree reasonably well with the measured results. This can provide a new method for analyzing the horizontal cyclic bearing characteristics of piles.

Keywords: pile; strain wedge model; cyclic *p–y* curve; strain accumulation model; soft clay

check for updates

Citation: Liu, X.; Yao, Z.; Zhu, W.; Zhang, Y.; Yan, S.; Guo, X.; Dai, G. A Simplified Calculation Method for Cyclic Response of Laterally Loaded Piles Based on Strain Wedge Model in Soft Clay. *J. Mar. Sci. Eng.* **2022**, *10*, 1632. https://doi.org/10.3390/jmse10111632

Academic Editor: Dong-Sheng Jeng

Received: 24 September 2022
Accepted: 27 October 2022
Published: 2 November 2022

1. Introduction

Cyclic loading not only weakens the strength and stiffness of soft clay around the pile, but also causes the excessive cumulative deformation of a single pile and reduces the lateral bearing capacity of the pile foundation. The *p–y* curve method is a practical method to calculate the horizontal bearing capacity of the pile foundation (Jeanjean [1], Kodikara et al. [2]), stiff clay (Reese and Welch [3], Sullivan et al. [4], Dunnavant and O'Neill [5]), and sand (Georgiadis [6]). Simultaneously, the *p–y* curve method was adopted in the American Petroleum Institute (API) [7] and Det Norske Veritas (DNV) [8] standards. API specification [9] suggests that the static *p–y* curve is taken as the backbone curve of the cyclic *p–y* curve by introducing the reduction coefficient of ultimate soil resistance to describe the cyclic weakening effect of the pile. However, this method has poor applicability to piles and seriously underestimates the cumulative deformation of the pile foundation. It is impossible to accurately predict the long-term cyclic deformation of the pile foundation.

A large-diameter single pile has a size effect, so the contribution of pile-side resistance, pile-top bending moment, and pile-top shear force should be considered in the bearing capacity design of a single pile. Byrne et al. [10] proposed a "four-spring" model to analyze the lateral bearing capacity of large-diameter rigid piles. Fu et al. [11] adopted the "double-spring" model to analyze the lateral bearing capacity of large-diameter rigid piles by considering the resistance of pile-side and pile-top soil. Wang et al. [12] introduced a rotating spring to represent the contribution of the following parts of the rotating point to the lateral bearing capacity, which is simplified into the p–y + M_R–θ_R double-spring model. The effectiveness of this method is verified by cases. Norris [13] proposed a strain wedge model to calculate the horizontal bearing capacity of the pile foundation. Based on the method, the shear strain of soil can be established to connect with the deflection of the pile foundation. Ashour et al. [14,15] proposed an improved strain wedge method to calculate the horizontal bearing characteristics of the pile foundation in multi-layer soil. Xu et al. [16]

proposed an improved strain wedge method by introducing the Duncan–Chang model [17] into the strain wedge model. Yang et al. [18] established an improved strain wedge method by considering the nonlinear deformation of a pile. Peng et al. [19] proposed an upper soil wedge and a modified lower strain wedge for the analysis of laterally loaded piles on sloping ground, and Zhu et al. [20] proposed a simplified calculation method for analyzing the long-term deformation of the suction caisson foundation in the soft clay under cyclic lateral loading.

In order to analyze the horizontal circulation effect of large-diameter single piles, this paper proposed a simplified calculation method based on the modified strain wedge model. Based on the concept of the secant stiffness attenuation, a stiffness attenuation model is proposed to describe the cyclic p–y curve for analyzing the cyclic bearing characteristics of piles in soft clay. Furthermore, the simplified calculation method for the horizontal cyclic effect of a single pile was verified by two case studies. This can provide a new method for analyzing the horizontal cyclic bearing characteristics of piles.

2. Large-Diameter Single Pile Cyclic Response Calculation Model

2.1. Simplified Calculation Model

In order to analyze the lateral circulation effect of large-diameter single piles, this paper adopts the p–y + M_R–θ_R double-spring model, which was proposed by Wang et al. [12] and Yi et al. [21]. As shown in Figure 1, L is the buried depth of the pile, L_e is the pile length above the rotating point, D is the diameter of the pile, and H is the pile length below the rotating point. The pile–soft clay interaction above the rotating point is represented by the p–y curve, and the pile–soft clay interaction below the rotating point is represented by the equivalent rotation spring. The modified strain wedge method is used to construct the p–y curve above the rotating point by considering the continuity and nonlinearity of soft clay. The soil resistance below the rotational point is equivalent to the M_R–θ_R model of the rotational point. The hyperbolic function is used to express the relationship between the rotational anti-torque M_R and the rotational angle θ_R. Finally, the stiffness attenuation model is proposed to calculate the lateral bearing capacity and deformation performance of the pile foundation by considering the cyclic stiffness attenuation and strength weakening of soft clay. The simplified calculation method is related to normally consolidated clays. The modified strain wedge model, M_R–θ_R model, and stiffness attenuation model are introduced in the following sections.

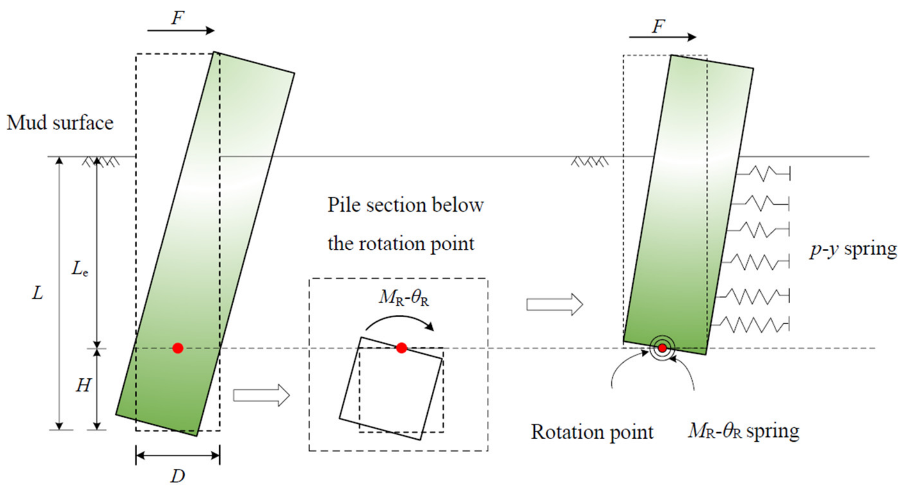

Figure 1. Simplified calculation model.

2.2. Strain Wedge Model

Norris [13] and Ashour et al. [14] proposed that the passive wedge deformation in front of piles can be simplified by a three-dimensional wedge shape mode. The wedge geometric shape can be represented by the base angle β_m, the fan angle φ_m, and the maximum depth

h (see Figure 2). As the lateral loading gradually increases, the wedge size and the stress and strain of the wedge also increase. In addition, the fan angle of the wedge is related to the effective internal friction angle. When the strength of the soft clay reaches the ultimate failure, the fan angle reaches its maximum value. Then, the base angle β_m and the wedge width ($\overline{BC}$) at any depth z can be defined as follows:

$$\beta_m = 45^\circ + \frac{\varphi_m}{2} \tag{1}$$

$$\overline{BC} = D + 2(H - z)\tan\beta_m \tan\varphi_m \tag{2}$$

where D is the width (or diameter) of the pile cross-section, φ_m denotes the fan friction angle (°), β_m denotes the base angle of the wedge layer (°), z denotes the pile depth from the ground (m), D denotes the pile width (m), and H denotes the mobilized depth from the ground (m).

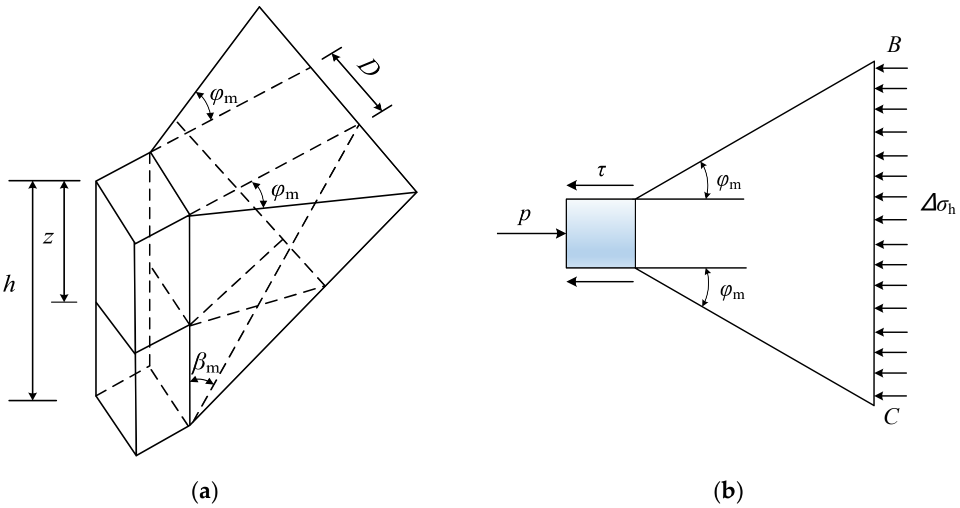

Figure 2. Strain wedge model: (**a**) three-dimensional view; (**b**) plan view.

The resistance of the wedge layer can be expressed as follows:

$$p = \Delta\sigma_h \overline{BC} S_1 + 2\tau D S_2 \tag{3}$$

where p denotes the soil reaction (kN/m), $\Delta\sigma_h$ denotes the horizontal stress change (kPa), τ_i denotes the shear stress (kPa), and S_1 and S_2 denote the shape coefficients.

The ultimate resistance of soft clay can be calculated as follows:

$$p_u = (\eta 10 s_u + \xi 2 s_u)D \tag{4}$$

where η and ξ represent the shape coefficients of the pile. For a circular pile, η = 0.75, ξ = 0.5, and for a square pile, η = ξ = 1.0.

In this study, the hyperbolic model is adopted to analyze the stress–strain relationship (see Figure 3). The initial confining pressure is assumed to be $s_h = K_0 s_v = s_3$. The effective major principal stress is assumed to be $\sigma_h + \Delta\sigma_h = \sigma_1$. In the ith wedge layer, the horizontal stress can be expressed as follows:

$$(\Delta\sigma_h)_i = (\sigma_1 - \sigma_3)_i = \frac{\varepsilon_i}{\frac{1}{E_{si}} + \frac{\varepsilon_i}{(\sigma_1 - \sigma_3)_{ulti}}} \tag{5}$$

where ε represents axial strain in the triaxial test, corresponding to the lateral strain in wedge body; $(\sigma_1 - \sigma_3)$ is the deviatoric stress in the triaxial test, corresponding to the lateral stress increment $\Delta\sigma_h$ within the wedge; $(\sigma_1 - \sigma_3)_{ult}$ is the asymptotic value of the deviational stress; and E_{si} is the initial secant modulus, which can be calculated [22] as follows:

$$E_{si} = \frac{2R_f s_u}{\varepsilon_{50}(2R_f - 1)} \tag{6}$$

where R_f is the stress failure ratio, usually ranging from 0.75 to 1.0, s_u is the undrained shear strength; and ε_{50} is the axial strain corresponding to one-half the deviatoric stress at ultimate failure.

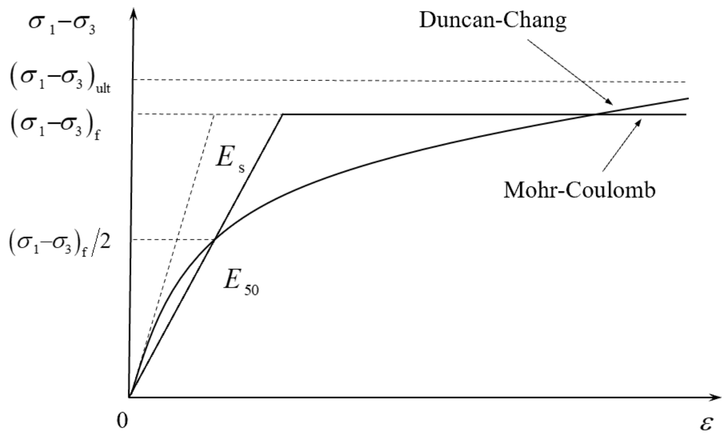

Figure 3. Hyperbolic model.

Based on the Coulomb–Mohr failure rules, the ultimate strength of the soft clay in the *i*th wedge layer can be obtained as follows:

$$(\sigma_1 - \sigma_3)_{ulti} = \frac{(\sigma_1 - \sigma_3)_{fi}}{R_f} \tag{7}$$

where $(\sigma_1 - \sigma_3)_{fi}$ is the failure strength (kPa), and $(\sigma_1 - \sigma_3)_{ulti}$ is the asymptotic failure strength (kPa).

The stress level SL can be written as follows:

$$SL = \frac{\Delta\sigma_h}{\Delta\sigma_{hf}} = \frac{\tan^2(\pi/4 + \varphi'_m/2) - 1}{\tan^2(\pi/4 + \varphi'/2) - 1} \tag{8}$$

To obtain the friction angle φ'_m, Ashour et al. [14] suggested establishing the relationship between the lateral stress increment ($\Delta\sigma_h$) and the exerted effective friction angle (φ') by the stress level SL.

Ashour et al. [15] and Xu et al. [16] introduced the hyperbolic model to characterize the variation characteristics of pile lateral shear stress. The pile–soft clay shear stress can be expressed as follows:

$$\tau = \frac{\Delta}{\frac{1}{k_s} + R_f \frac{\Delta}{\tau_f}} \tag{9}$$

where Δ is the relative displacement of pile–soft clay interface; R_f is the failure ratio; and k_s is the initial shear stiffness, which can be determined as follows:

$$k_s = \frac{\tau_{ult}}{\Delta_u} \tag{10}$$

where Δ_u is the ultimate displacement.

According to the Coulomb friction formula, τ_{ult} can be expressed as follows:

$$\tau_{ult} = c_{inter} + \sigma_n \tan\delta_{inter} \tag{11}$$

where σ_n is the normal stress at the pile–soft clay interface, and c_{inter} and δ_{inter} are interface cohesion and friction angle.

Ashour et al. [14] established the relationship between the deflection angle of the pile foundation δ and the shear strain γ. The relationship between the pile deflection and the strain of the wedge as follows:

$$\delta = \frac{\gamma}{2} \tag{12}$$

According to the Mohr circle of strain, the relationship between the shear strain and strain of soft clay can be expressed as follows:

$$\frac{\gamma}{2} = \frac{\gamma_{\max}}{2}\sin 2\theta_m = \frac{(1+\mu)\varepsilon}{2}\cos\varphi_m \tag{13}$$

where ε is the horizontal strain of soil, and μ is Poisson's ratio.

As shown in Figure 4, the relationship between the angle and displacement of the pile in the ith wedge layer can be expressed as follows:

$$\tan\delta_i = \frac{y_{i-1} - y_i}{h} \tag{14}$$

where y_{i-1} is the upper horizontal displacement of the pile element in the ith wedge layer, y_i is the bottom horizontal displacement of the pile element in the ith wedge layer, and h is the height of the pile element.

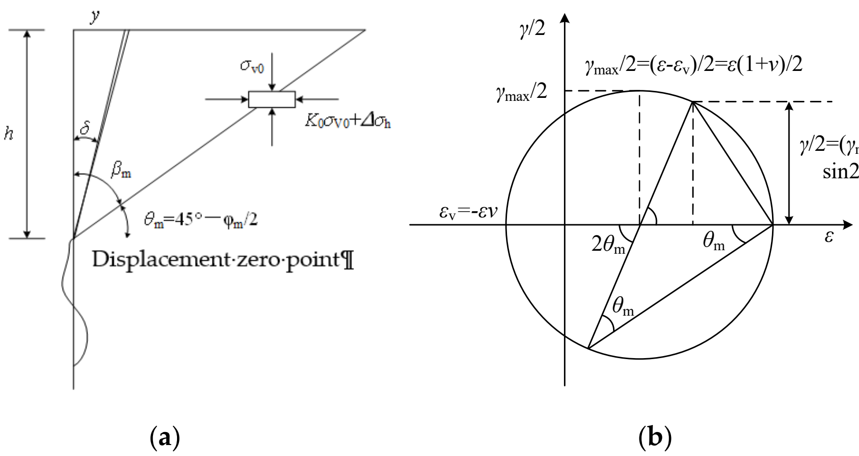

Figure 4. Displacement–strain relationship: (**a**) horizontal deformation mode; (**b**) Mohr circle of strain.

2.3. M_R–θ_R Model

Wang et al. [12] established M_R–θ_R relationship via the hyperbolic tangent function. Subsequently, Yi et al. [21] established the conversion relationship between the stress–strain of soft clay and M_R–θ_R. Therefore, the hyperbolic function is introduced to describe the relationship between the rotational anti-torque M_R and the rotation angle θ_R. The rotational anti-torque can be expressed as follows:

$$M_R = \frac{\theta_R}{\frac{1}{k_R} + \frac{\theta_R}{M_{R,ult}}} \tag{15}$$

where k_R is the initial rotational stiffness, and $M_{R,ult}$ is the ultimate rotational resistance moment.

The rotation of a rigid caisson is similar to the partial rotation of a rigid pile at the lower part of the rotational point. Under semi-infinite boundary conditions, the initial rotational stiffness k_R can be expressed as follows:

$$k_R = \frac{GD^3}{3(1-\mu)}\left[1+1.9\frac{H}{D}\left(1+\frac{2H}{D}\right)^{1.4}\right] \tag{16}$$

Yi et al. [21] proposed that the soft clay below the rotation point is the rotating failure model around the rotation point. The expression of the ultimate rotational resistance moment can be expressed as follows:

$$M_{R,ult} = M_{R,c} + M_{R,s} \tag{17}$$

where $M_{R,c}$ is the resisting moment due to sliding failure, and $M_{R,s}$ is the resisting moment caused by shear failure.

It is assumed that the undrained shear strength (s_u) of soft clay below the rotational point varies linearly along the depth. $S_u = s_{u0} + kz$, s_{u0} is the undrained shear strength at the rotational point, and k is the gradient of strength along the depth. The resistance moment $M_{R,c}$ can be expressed as follows:

$$\begin{aligned} M_{R,c} &= 4\int_0^{D/2}\int_0^{\pi/2}(s_{u0}+kr_c\sin\alpha)\cdot r_c\cdot r_c d\alpha dy \\ &= \left(\tfrac{1}{6}\pi D^3 s_{u0}+\pi s_{u0}DH^2\right)+k\left(\tfrac{1}{2}D^2+2H^2\right)^2\left[\tfrac{3}{8}t+\tfrac{1}{4}\sin 2t+\tfrac{1}{32}\sin 4t\right] \end{aligned} \tag{18}$$

where $t = \arcsin\left(\frac{D}{\sqrt{D^2+4H^2}}\right)$.

It can be obtained by introducing the shape correction coefficient r_s to the circular section's resistance moment. The resistance moment can be expressed as follows:

$$M_{R,s} = 4\int_0^H\int_0^{\pi/2} r_s(s_{u0}+kz\sin\varphi)\cdot z^2 d\varphi dz = 0.73\left(\frac{2\pi}{3}s_{u0}H^3+kH^4\right) \tag{19}$$

As shown in Figures 5 and 6, a three-dimensional hemispherical sliding surface is formed below the rotating point. A micro-element segment dl is taken to calculate distance r_c by the force balance on the sliding zone CBB′C′. The distance r_c can be expressed as follows:

$$r_c = O'B = \sqrt{(O'A)^2+(AB)^2} = \sqrt{(O'A)^2-(O'O)^2+(AB)^2} = \sqrt{\frac{D^2}{4}-y^2+H^2} \tag{20}$$

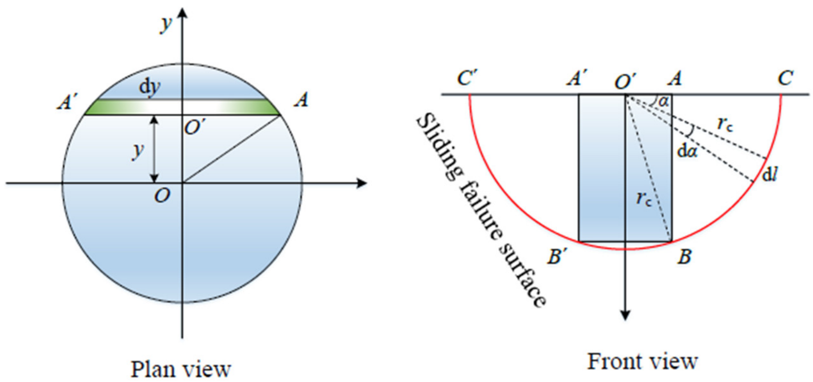

Figure 5. Sliding failure resistance moment.

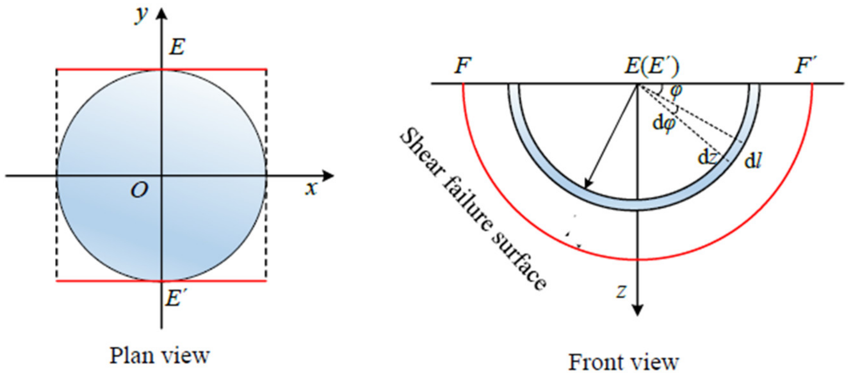

Figure 6. Shear failure resistance moment.

The ultimate rotational resistance moment $M_{\mathrm{R,ult}}$ is expressed as follows:

$$M_{\mathrm{R,ult}} = \left(\frac{1}{6}\pi D^3 s_{\mathrm{u0}} + \pi s_{\mathrm{u0}} D H^2\right) + k\left(\frac{1}{2}D^2 + 2H^2\right)^2\left[\frac{3}{8}t + \frac{1}{4}\sin 2t + \frac{1}{32}\sin 4t\right] + 0.73\left(\frac{2\pi}{3}s_{\mathrm{u0}}H^3 + kH^4\right) \quad (21)$$

where $t = \arcsin\left(\frac{D}{\sqrt{D^2+4H^2}}\right)$.

$M_{\mathrm{R,ult}}$ can be expressed as follows:

$$M_{\mathrm{R,ult}} = \left(\frac{1}{6}\pi D^3 s_{\mathrm{u}} + \pi s_{\mathrm{u}} D H^2\right) + \frac{1.46\pi}{3} s_{\mathrm{u}} H^3 \quad (22)$$

2.4. Stiffness Attenuation Model

Saturated soft clay will show stiffness degradation and strength weakening under cyclic loading. Idriss et al. [23] and Yasuhara et al. [24] proposed an empirical model that can express the cyclic cumulative strain and stiffness attenuation of soil. This model is widely used to calculate the lateral cyclic loading effect analysis of a single pile.

As shown in Figure 7, Idriss et al. [23] defined the shear modulus degradation index ζ to represent the strength-weakening degree of clay. The cyclic degradation index can be expressed as follows:

$$\zeta = \frac{G_{\mathrm{sN}}}{G_{\mathrm{s1}}} = \frac{\frac{\sigma_d}{\varepsilon^N}}{\frac{\sigma_d}{\varepsilon^1}} = \frac{\varepsilon^1}{\varepsilon^N} \quad (23)$$

where σ_{d} is the amplitude of cyclic stress; G_{s1} and G_{sN} are the cyclic shear modulus of the 1st and Nth loading, respectively; and ε^1 and ε^{N} are the lateral strain of soft clay at the 1st and Nth loading to the peak, respectively.

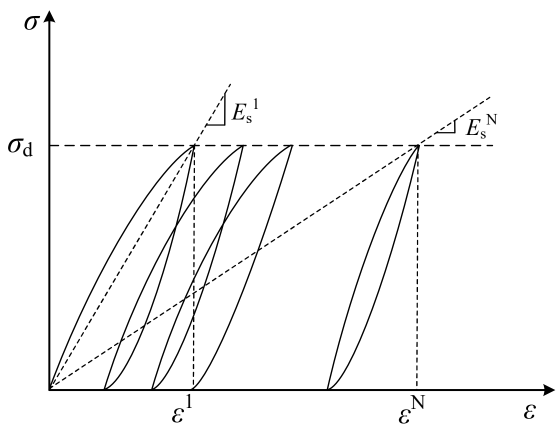

Figure 7. Decay curve of secant elastic modulus in clay.

Idriss et al. [23] point out that the attenuation exponent ζ is exponentially dependent on the number of cycles N. The attenuation exponent is expressed as follows:

$$\zeta = N^{-t} \tag{24}$$

Contrastively, Yasuhara et al. [24] proposed an attenuation exponent, which is expressed as follows:

$$\zeta = 1 - d\lg N \tag{25}$$

where d is the softening parameter related to the cyclic stress level, which can be calculated by the following formula:

$$d = \lambda r_s^2 \tag{26}$$

where λ is the parameter related to types of soil, and r_s is the cyclic stress ratio.

Li and Huang [25] proposed the relationship between attenuation index ζ expressed in natural logarithm and cycle number N for marine clays. The attenuation index is expressed as follows:

$$\zeta = 1 - d \ln N \tag{27}$$

This paper established the stiffness attenuation model by considering the influence factor, which includes the number of cycles, cyclic stress level, and loading frequency. The stiffness attenuation model is expressed as follows:

$$\zeta = 1 - (ar_s + b) f^c \ln N \tag{28}$$

where f is the loading frequency; and a, b, and c are the fitting parameters, which can be determined from the laboratory dynamic triaxial test data of soft clay.

2.5. Calculation Method and Program Implementation

This paper adopts the finite difference method to solve the pile–soft clay interaction. Firstly, the pile is equally divided into n elements, the length of each element is h, and the number of each element is shown in Figure 8. For the convenience of calculation, two virtual equal points are added at the pile top and the pile end, respectively. Then, the corresponding differential equation of the pile foundation deflection can be obtained as follows:

$$EI\frac{d^4 y_i}{dz^4} + E_{si} y_i = 0 \tag{29}$$

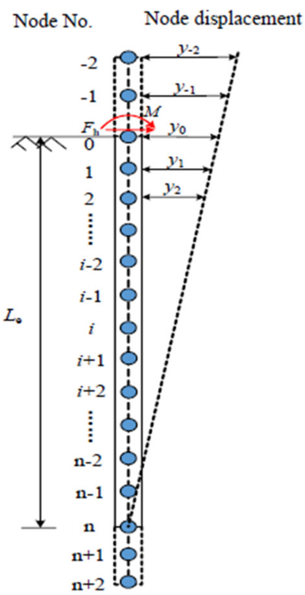

Figure 8. Node Number.

It is assumed that the top of the pile is a free boundary, which is subjected to lateral loading H_0 and bending moment M_0. The lateral displacement at the rotation point is y_R, and the rotational bending moment is M_R.

$$\begin{cases} EIy''|_{z=0} = M_0 \\ EIy'''|_{z=0} = H_0 \\ y|_{z=L_e} = 0 \\ EIy''|_{z=Le} = M_R \end{cases} \quad (30)$$

Based on the deflection differential equation of the pile foundation and boundary conditions, the displacement matrix equation is established as follows:

$$[K]\{y\} = \{F\} \quad (31)$$

where $\{F\}$ is the column vector of external loading, $\{y\}$ is the column vector of the pile foundation displacement, and $[K]$ is the lateral stiffness matrix.

The solution steps for horizontal loading of a single pile under cyclic loading are as follows:

(1) Input the corresponding physical parameters and loads, assume that the initial value of the lateral displacement of the pile head at the mud surface is y_0, and the displacement of each node is $y_i = y_0(n-i)/n$, where $1 \leq I \leq n$;

(2) For each layer, the initial tangent modulus E_{ini}, the ultimate deviatoric stress $(\sigma_1–\sigma_3)_{ult}$, and the excess pore water pressure Δu are calculated from Equations (6) to (8), respectively;

(3) Eliminate ε_i from Equations (5), (12), and (14), iteratively calculate the developed internal friction angle φ'_m, and then obtain the $\Delta\sigma_{hi}$ and ε_i of each layer;

(4) Calculate τ_i of each layer from Equations (9)–(11), and calculate the resistance p_i of each layer from Equation (3);

(5) Calculate the ultimate soil resistance p_u from Equation (4), and determine the relationship between p_i and p_u. If $p_i \geq p_u$, make $p_i = p_u$, then calculate the modulus of the foundation reaction of each sublayer E_{si};

(6) Calculate the initial rotational stiffness k_R and the ultimate rotational torque $M_{R,ult}$ at the rotational point from Equations (16), (21), or (22), respectively, and then examine the rotational torque M_R at the rotational point from Equation (15);

(7) Combined with the boundary conditions of Equation (29), construct the stiffness matrix $[K]$, calculate the lateral displacement $\{y\}$ of the pile from Equation (30), and judge that $|y-y_0| \leq 10^{-5}$. If the calculated data are saved, they will be used as the water level strain after the first cyclic loading lateral strain ε^1 and lateral stress increment $\Delta\sigma_h{}^1$, namely, cyclic stress σ_{cyc}. Conversely, let $y_0 = y$ and repeat steps (2)–(6);

(8) The attenuation indices ζ and t of soft clay are calculated from Equation (28), and the lateral strain ε_N of each sublayer under the peak stress σ_{cyc} under the Nth cyclic loading is calculated by Equations (30) and (31). Furthermore, the lateral stiffness k value under the Nth cyclic loading can be derived;

(9) Repeat Steps (2)–(7) to calculate the internal force and deformation of the pile after the Nth cycle. The program calculation flow chart is shown in Figure 9.

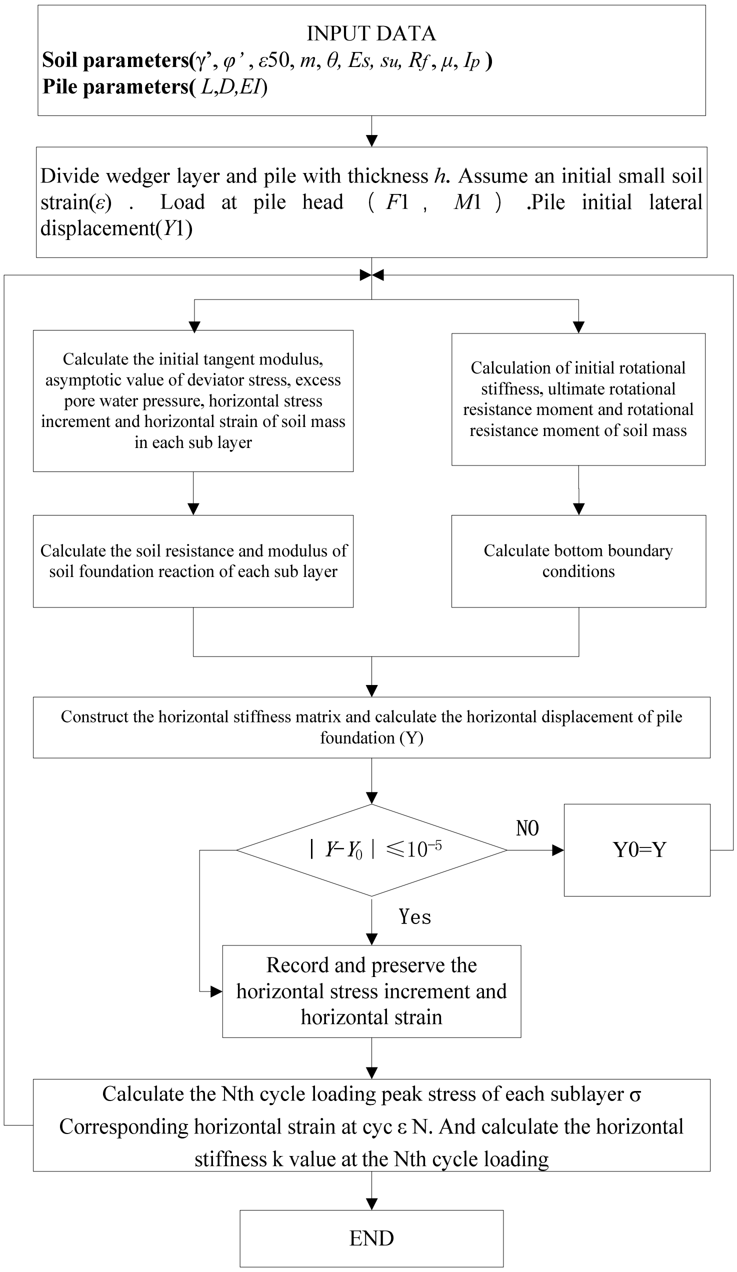

Figure 9. Flow chart for calculation.

3. Method Validation

3.1. Case 1

Murali et al. [26] carried out a centrifuge test of rigid piles under lateral loading in normal consolidated soft clay. The test pile diameter D was 3.72 m, the effective embedding depth L was 7.62 m, the aspect ratio L/D was 2.05, the wall thickness t was 0.045 m, and the flexural rigidity EI was 31.2 GN·m^2. The lateral loading points above the mud surface were 1.25 and 3.5, respectively. The undrained shear strength of the soils was $s_u = 1 + 1.1\,z$. The lateral loading point above the mud surface was 1.5 and 2.5, respectively. The undrained shear strength of the soils was $s_u = 1 + 1.3\,z$. The soft clay was prepared from saturated kaolin, where the saturation weight γ_{sat} was 15.5 kN/m^3, the liquid limit was 63%, and the plasticity index was 33%.

Figure 10 shows the loading–displacement curves of the measured and calculated values at the mud surface. It can be seen that the displacement nonlinearly increases as the loading increases gradually. The height of the loading point has a significant effect on the lateral bearing capacity of large-diameter single piles. The larger the height of the loading point, the smaller the lateral bearing capacity. The results from the present method agree reasonably well with the measured results, which indicate that the simplified calculation model proposed can be applied to calculate the lateral bearing capacity of large-diameter rigid piles.

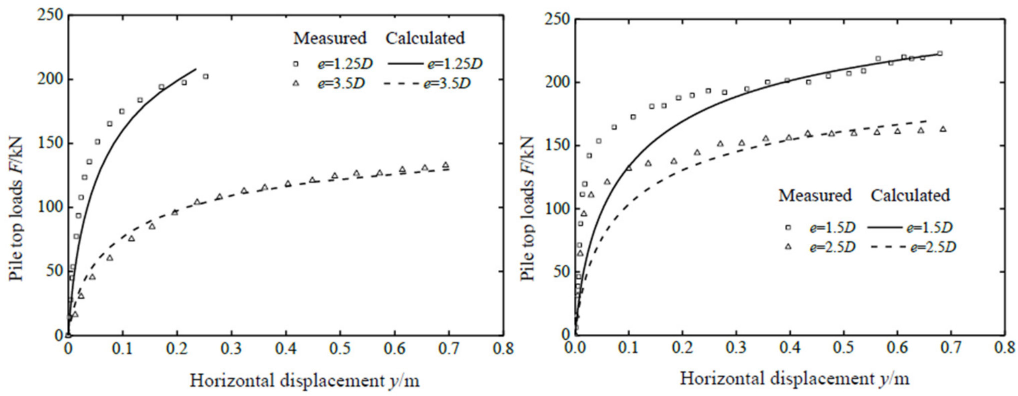

(**a**) (**b**)

Figure 10. Comparison of load–displacement curves. (**a**) $s_u = 1 + 1.1\,z$, (**b**) $s_u = 1 + 1.3\,z$.

3.2. Case 2

Yang et al. [27] presented a horizontal cyclic bearing characteristic centrifuge test of the pile foundation. The pile diameter D was 5.9 m, the wall thickness t was 0.062 m, the effective embedding depth L was 55 m, and the bending stiffness EI was 1097.25 GN·m^2, the rotation point was 0.75 L. The soft clay was prepared from Malaysian kaolin, the saturated weight γ_{sat} was 15.5–16.4 kN/m^3, the liquid limit was 80%, the plasticity index was 45%, and the friction angle φ was 23°. The undrained shear strength of soft clay after consolidation was s_u = 1.26 z. The cyclic loading height was 23 m, the loading frequency was 0.2 Hz, and the cyclic loading amplitudes were 0.25–1.0 MN (C2-1), 0.45–1.75 MN (C2-2), and 0.45–3.7 MN (C2-3), respectively, while the cycles were 100, 100, and 180, respectively.

Figure 11 shows the comparison results between the measured and calculated values of pile lateral displacement. It can be seen from the figure that under different cycle numbers, the variation trend of the lateral displacement of the pile body along the depth is the same. The lateral displacement gradually increases with the increase in cycle numbers. Furthermore, the results from the present method agree reasonably well with the measured results. Figure 12 shows the comparison results between the measured and the calculated value of the pile bending moment. It can be seen from the figure that the variation trend of the pile bending moment along the depth is roughly the same under different cycle numbers. With the increase in cycle number, the pile bending moment gradually increases. Additionally, the maximum bending moment occurs at the same location. The calculated values of the maximum bending moment are close to the measured values. Thus the simplified calculation model can better predict the internal force and the deformation of the pile better.

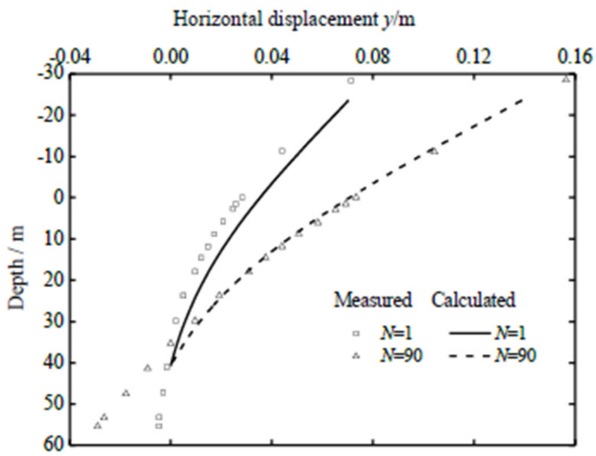

(a) C2-1

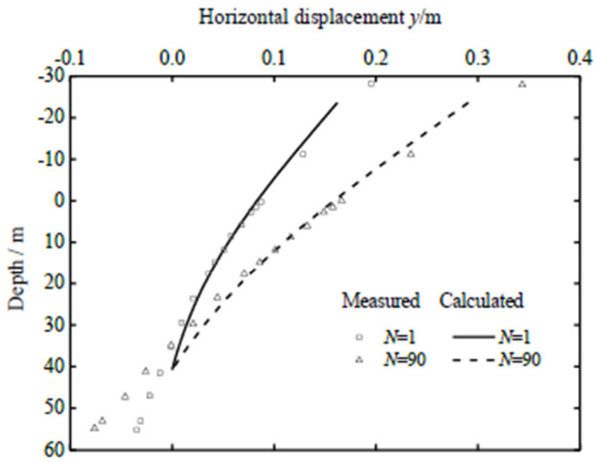

(b) C2-2

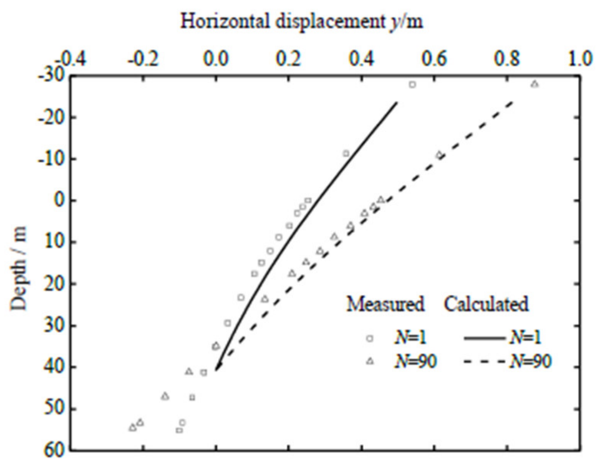

(c) C2-3

Figure 11. Comparisons of cyclic horizontal displacements.

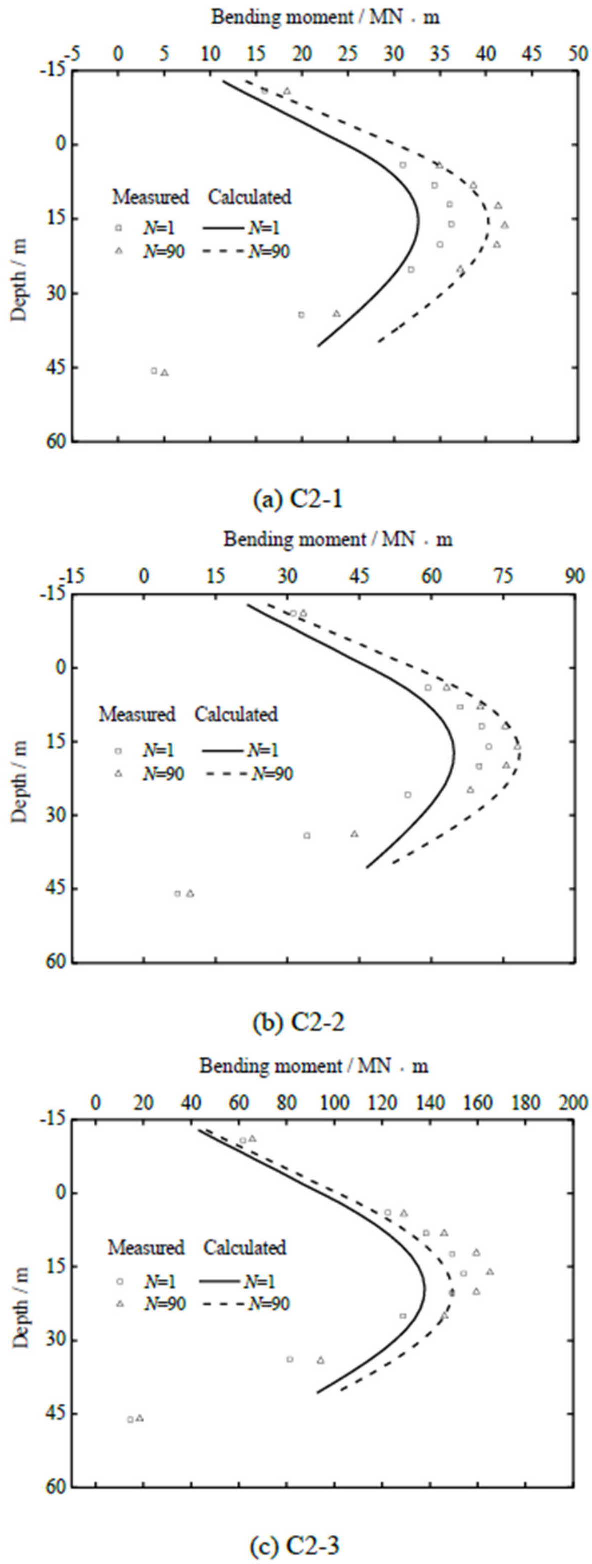

Figure 12. Comparison of cyclic bending moment.

4. Conclusions

This paper proposes a simplified calculation method based on the modified strain wedge model, which can effectively analyze the horizontal bearing characteristics of piles. In addition, the effectiveness of the method is verified by two numerical examples. The main conclusions can be summarized as follows:

(1) Based on the strain wedge model, the soil resistance below the rotation point is equivalent to the rotation spring. A simplified calculation model for the horizontal bearing capacity of large-diameter single piles in saturated soft clay is established based on the improved strain wedge model.

(2) A stiffness attenuation factor was established to describe the cyclic *p*–*y* curve for analyzing the cyclic bearing characteristics of soil. At the same time, a stiffness attenuation factor is applied to the simplified calculation model for analyzing the cyclic *p*–*y* curve and the cyclic bearing characteristics of piles.

(3) Two case studies are described to verify the reliability and accuracy of the simplified calculation model. The results from the present method agree reasonably well with the measured results, which can verify the effectiveness of the simplified calculation model. It can provide a new method for analyzing the horizontal cyclic bearing characteristics of piles.

Author Contributions: Conceptualization, methodology, validation, formal analysis, investigation, data curation, writing—original draft, visualization, X.L.; formal analysis, investigation, data curation, Z.Y.; investigation, resources, data curation, writing—review and editing, project administration, W.Z.: investigation, resources, writing—review and editing, supervision, project administration, funding acquisition, Y.Z.; writing—review and editing, S.Y.; writing—review and editing, X.G.; investigation, resources, data curation, project administration, G.D. All authors have read and agreed to the published version of the manuscript.

Funding: This work was supported by the Science and Technology program of China Huaneng Group (HNKJ20-H53), the National Natural Science Foundation of China (Grant Numbers: 52208333, 51878160, and 52078128), the Jiangsu Province Excellent Postdoctoral Funding Program (Grant Number: 2022ZB135), the Postdoctoral Innovation Talent Fund (Grant Number: 2242022R20025), and the Technology Project of China Huaneng Group Co., Ltd. (Grant Number: HNKJ19-H17).

Institutional Review Board Statement: Not applicable.

Informed Consent Statement: Not applicable.

Data Availability Statement: The data used to support the findings of this study are included within the article.

Acknowledgments: The authors thank the Big Data Center of Southeast University for providing the facility support on the numerical calculations in this paper.

Conflicts of Interest: The authors declare no conflict of interest.

References

1. Jeanjean, P. Re—assessment of p–y curves for soft clays from centrifuge testing and finite element modeling. In Proceedings of the Offshore Technology Conference, Paper No. OTC 20158, Houston, TX, USA, 4–7 May 2009; pp. 1–23.
2. Kodikara, J.; Haque, A.; Lee, K.Y. Theoretical p-y Curves for Laterally Loaded Single Piles in Undrained Clay Using Bezier Curves. *J. Geotech. Geoenviron. Eng.* **2010**, *136*, 265–268. [CrossRef]
3. Reese, L.C.; Welch, R.C. Lateral Loading of Deep Foundations in Stiff Clay. *J. Geotech. Eng. Div.* **1975**, *101*, 633–649. [CrossRef]
4. Sullivan, W.R.; Reese, L.C.; Fenske, C.W. Unified Method for Analysis of Laterally Loaded Piles in Clay. In *Numerical Methods in Offshore Piling*; Institution of Civil Engineers: London, UK, 1980; pp. 135–146.
5. Dunnavant, T.W.; O'Neill, M.W. Experimental p–y model for submerged stiff clay. *J. Geotech. Eng.* **1989**, *115*, 95–114. [CrossRef]
6. Georgiadis, M.; Anagnostopoulos, C.; Saflekou, S. Centrifugal testing of laterally loaded piles in sand. *Can. Geotech. J.* **1992**, *29*, 208–216. [CrossRef]
7. API. *Geotechnical and Foundation Design Considerations, ANSI/API Recommended Practice 2 GEO*, 1st ed.; API: Washington, DC, USA, 2011.
8. DNV. Design of Offshore Wind Turbine Structures. In *Recommended Practice DNV–RP–H103*; Det Norske Veritas: Baerum, Norway, 2011.
9. American Petrolem Institute. *Recommended Practice for Planning Designing and Constructing Fixed Offshore Platforms-Working Stress Design*; American Petroleum Institute Publishing Services: Washington, DC, USA, 2005.
10. Byrne, B.W.; Houlsby, G.T.; Burd, H.J.; Gavin, K.G. PISA design model for monopiles for offshore wind turbines: Application to a stiff glacial clay till. *Géotechnique* **2020**, *70*, 1030–1047. [CrossRef]

11. Fu, D.F.; Zhang, Y.H.; Aamodt, K.K.; Yan, Y. A multi-spring model for monopiles analysis in soft clay. *Mar. Struct.* **2020**, *72*, 102768. [CrossRef]
12. Wang, L.Z.; Lai, Y.Q.; Hong, Y.; Maín, D. A unified lateral soil reaction model for monopiles in soft clay considering various lengt-to-diameter (L/D) ratios. *Ocean. Eng.* **2020**, *212*, 107492. [CrossRef]
13. Norris, G.M. Theoretically based BEF laterally loaded pile analysis. In Proceedings of the 3rd International Conference on Numerical Methods in Offshore Piling, Nantes, France, 21–22 May 1986; pp. 361–386.
14. Ashour, M.; Norris, G.; Pilling, P. Lateral loading of a pile in layered soil using the strain wedge model. *J. Geotech. Geoenviron. Eng.* **1998**, *124*, 303–315. [CrossRef]
15. Ashour, M.; Norris, G. Modeling lateral soil–pile response based on soil–pile interaction. *J. Geotech. Geoenviron. Eng.* **2000**, *126*, 420–428. [CrossRef]
16. Xu, L.; Cai, F.; Wang, G.X.; Ugai, K. Nonlinear analysis of laterally loaded single piles in sand using modified strain wedge model. *Comput. Geotech.* **2013**, *51*, 60–71. [CrossRef]
17. Duncan, J.M.; Chang, C.Y. Nonlinear analysis of stress and strain in soils. *J. Soil. Mech. Found. Div.* **1970**, *96*, 1629–1653. [CrossRef]
18. Yang, X.; Zhang, C.; Huang, M.S.; Yuan, J.Y. Lateral loading of a pile using strain wedge model and its application under scouring. *Mar. Geo. Geotech.* **2017**, *6*, 340–350. [CrossRef]
19. Peng, W.; Zhao, M.; Xiao, Y.; Yang, C.W.; Zhao, H. Analysis of laterally loaded piles in sloping ground using a modified strain wedge model. *Comput. Geotech.* **2019**, *107*, 163–175. [CrossRef]
20. Zhu, W.B.; Dai, G.L.; Wang, B.C.; Gong, W.M.; Sun, J.; Hu, H. Study on cyclic characteristics and equivalent cyclic creep model of the soft clay at the bottom of suction caisson foundation. *Rock Soil Mech.* **2022**, *43*, 466–478.
21. Yi, B.; Lw, B.; Yz, A.; Yi, H.B. Site-specific soil model for monopiles in soft clay based on laboratory element stress-strain curves. *Ocean. Enineering* **2021**, *220*, 108437.
22. Brinkgreve, R.B.J. *Plaxis User's Manual-Version 8*; Balkema: Rotterdam, The Netherlands, 2002.
23. Idriss, I.M.; Singh, R.D.; Dobry, R. Nonlinear behavior of soft clays during cyclic loading. *J. Geotech. Eng. Div.* **1978**, *104*, 1427–1447. [CrossRef]
24. Yasuhara, K.; Hyde, A.F.L.; Toyota, N. Cyclic stiffness of plastic silt with an initial drained shear stress. In *Pre-Failure Deformation of Geoterials*; Thomas Telford Ltd.: London, UK, 1998; pp. 373–382.
25. Li, S.; Huang, M.S. Undrained long-term cyclic degradation characteristics of offshore soft clay. In *Soil Dynamics and Earthquake Engineering*; ASCE: Reston, VA, USA, 2010; pp. 263–271.
26. Murali, M.; Hrajales-Saavedra, F.J.; Beemer, R.D.; Aubeny, C.P.; Biscontin, G. Capacity of short piles and casissons in soft clay from geotechnical centrifuge tests. *J. Geotech. Geoenviron. Eng.* **2019**, *145*, 04019079. [CrossRef]
27. Yang, Q.J.; Gao, Y.F.; Kong, D.Q.; Zhu, B. Centrifuge modelling of lateral loading behavior of a "semi-rigid" monopile in soft clay. *Mar. Georesources Geotechnol.* **2019**, *37*, 1205–1216. [CrossRef]